



Evaluating snow depth measurements from ground-penetrating radar and airborne lidar in boreal forest and tundra environments during the NASA SnowEx 2023 campaign

Kajsa Holland-Goon¹, Randall Bonnell^{2,1}, Daniel McGrath¹, W. Brad Baxter³, Tate Meehan⁴, Ryan Webb⁵, Christopher F. Larsen⁶, Hans-Peter Marshall⁷, Megan Mason^{8,9}, and Carrie Vuyovich⁸

¹Department of Geosciences, Colorado State University, Fort Collins, Colorado, USA

²U.S. Geological Survey, Water Resources Mission Area, Denver, Colorado, USA

³Cold Regions Research and Engineering Laboratory, U.S. Army Corps of Engineers, Fairbanks, Alaska, USA

⁴Cold Regions Research and Engineering Laboratory, U.S. Army Corps of Engineers, Hanover, New Hampshire, USA

⁵Department of Civil and Architectural Engineering & Construction Management, University of Wyoming, Laramie, Wyoming, USA

⁶Geophysical Institute, University of Alaska, Fairbanks, Alaska, USA

⁷Department of Geosciences, Boise State University, Boise, Idaho, USA

⁸Hydrological Sciences Laboratory, NASA Goddard Space Flight Center, Greenbelt, Maryland, USA

⁹Science Systems Applications Inc., Lanham, Maryland, USA

Correspondence: Randall Bonnell (rbonnell@usgs.gov) and Daniel McGrath (daniel.mcgrath@colostate.edu)

Received: 23 May 2025 – Discussion started: 1 August 2025

Revised: 13 January 2026 – Accepted: 10 March 2026 – Published: 17 April 2026

Abstract. Snow is a vital component of high-latitude terrestrial systems, but environmental factors (e.g., permafrost) and complex vegetation challenge the accurate measurement of key snowpack properties. We evaluated local-scale ground-penetrating radar (GPR) and large-scale airborne lidar retrievals of snow depth collected during the NASA SnowEx 2023 campaign in tundra and boreal forest environments in Alaska along 44 short (3–12 m) transects. Compared to in situ observations, we identified modest biases for GPR snow depths (bias < 0.03 m in tundra, +0.06 m in boreal forests) and larger biases for lidar snow depths in the boreal forests (−0.16 m). At the Upper Kuparuk-Toolik tundra site, lidar snow depths exhibited a small bias (−0.02 m), whereas the bias was much larger at the Arctic Coastal Plain tundra site (+0.19 m). For most sites, biases were primarily related to sub-snow vegetation, tussocks, and seasonally dynamic ground. However, we identified vertical alignment issues with the Arctic Coastal Plain lidar snow depth dataset that likely contributed to the higher bias. The complex ground surface and sub-snow vegetation in these environments present a challenge to established snow depth mea-

surement methods, which needs to be considered when evaluating novel remote sensing approaches.

1 Introduction

In high-latitude (> 60°) terrestrial systems, snow plays a crucial role in the hydrologic cycle and modulates the surface energy balance. Snow strongly impacts the ecology of these regions: snow influences caribou winter range selection (Durette, 1988; Pedersen et al., 2021) and vegetation phenology (Kelsey et al., 2021), and provides winter refuges for a diverse range of animals (Aitchison, 1987; Peczykowski et al., 2017). Since 1967, snow cover extent in the Arctic has experienced dramatic reductions, with satellites observing declines of −3.5 % and −13.4 % per decade in May and June, respectively (Meredith et al., 2019). Given the vast spatial scales and sparse in situ station network, remote sensing can play a critical role in snowpack monitoring in these sensitive environments.

The NASA SnowEx 2023 campaign was implemented to improve the understanding of remote sensing methods for retrievals of snow depth and snow water equivalent (SWE), the mass of the snowpack, in tundra and boreal forest environments (Vuyovich et al., 2024). These regions are understudied relative to temperate mountains; for instance, they are currently not included in gridded SWE analysis products (e.g., SNODAS). Space-borne remote sensing retrievals of snow depth or SWE at high spatial resolution may be achievable in these complex environments through lidar or radar methods (Fair et al., 2025; Eppler et al., 2022), but further evaluation of the uncertainties caused by the unique physical parameters within these environments (e.g., dense canopy cover and ground vegetation) is required.

The boreal forest is characterized by a dense canopy of coniferous and deciduous trees and covers 10%–17% of the world's landmass (NASA Earth Observatory, 2006; Vuyovich et al., 2024). Boreal forest seasonal snowpacks are typically shallow (< 1.2 m) and exhibit lower snow densities due to minimal wind loading, cold temperatures, and large temperature gradients in the snowpack, resulting in extensive faceting (Pruitt, 1970). In contrast, the Arctic tundra extends to higher latitudes than boreal forests and is subject to extreme cold temperatures and high winds that limit plant growth. Tundra snowpacks are typically shallower than boreal forest snowpacks, but wind redistribution can build deep snow drifts (Benson, 1967; Benson and Sturm, 1993). Because of wind-driven compaction, tundra snowpacks can exhibit higher densities than snowpacks in the boreal forest and include a binary stratigraphy of high-density wind slab above low-density, large-grained depth hoar. Both environments have features that may complicate snow depth retrievals from lidar or radar methods. In boreal forests, thick forest canopy, canopy-intercepted snow, and dense shrub and tussock (i.e., small localized tufts of grass or sedge where the solid ground is raised) cover may occlude lidar, whereas dense shrub cover can cause a void space between the bottom of the snowpack and the ground, leading to a mismatch between the more easily identified radar ground reflector and the true base of the snowpack. Tundra environments contain spatially varying distributions of shrub and tussock cover that may increase uncertainty of lidar or radar methods. Additionally, the North Slope tundra ground surface is complex and experiences seasonal fluctuations driven by freeze-thaw processes. These environments contain hummocks, ice wedges, ice polygons, and are underlain by shallow permafrost (Jorgensen et al., 2008). This dynamic ground surface can increase lidar snow depth uncertainty because of differences in the ground elevation between snow-on and snow-off lidar acquisitions (Chen et al., 2020). In both environments, frozen soil may have similar dielectric properties to the snowpack, and thus the radar signal can penetrate below the snow-ground interface.

During NASA SnowEx 2023 in Alaska, we conducted detailed in situ surveys to improve our understanding of radar

and lidar performance for snow depth retrieval in these complex high-latitude environments. Here, we evaluate ground-based radar and airborne lidar snow depth products along transects where manual measurements of snow depth were collected after snow excavation. The excavated snow depths represent the integrated thickness of the snowpack, which excludes intra- and sub-snowpack void spaces. In particular, we emphasize how sub-snow vegetation and variable ground conditions associated with mosses, tussocks, and/or permafrost influence the retrieval accuracy.

2 Study Sites

The NASA SnowEx 2023 Alaska campaign (7–16 March 2023) was operated at three field sites in the boreal forests near Fairbanks (Fig. 1a–c) and two sites in the Arctic tundra on the North Slope (Fig. 1d, e). Although some snowmelt was observed in the boreal forest canopy, the snowpack on the ground was considered dry based on snow pit temperature measurements. Of the boreal forest sites, the Caribou/Poker Creek Research Watershed site (CPCRW; Fig. 1a) is located ~ 25 km northeast of Fairbanks and hosted eight surveys, the Farmers Loop Experimental Station and Creamer's Field Migratory Waterfowl Refuge (FLCF; Fig. 1b) north of Fairbanks hosted six surveys, and the Bonanza Creek Experimental Forest (BCEF; Fig. 1c) is ~ 20 km southwest of Fairbanks and hosted four surveys. Vegetation varied by site: CPCRW surveys were performed primarily below black spruce canopy, FLCF included transects within black spruce (*Picea mariana*), deciduous, mixed canopy, and agricultural field environments, and BCEF surveys were performed primarily below leaf-off deciduous canopy and in wetland shrub environments (Vuyovich et al., 2024). Surveys at the Upper Kuparuk-Toolik site (UKT; Fig. 1d) had ground conditions that varied from shrubs and tussocks to frozen ponds, whereas the Arctic Coastal Plain site (ACP; Fig. 1e), located near Deadhorse, primarily included surveys performed in wetlands and frozen ponds/lakes (Vuyovich et al., 2024). The sites near Fairbanks are within the discontinuous permafrost region (Jorgensen et al., 2008), whereas both UKT and ACP are underlain by continuous permafrost (Obu et al., 2019).

3 Methods

3.1 Summary of Field and Airborne Lidar Surveys

We operated four ground-penetrating radar (GPR) systems to cover the five field sites, including two surface-coupled 1.0 GHz center-frequency PulseEkko Pro single transceiver/receiver systems, an air-coupled 1.0 GHz center-frequency PulseEkko Pro single transceiver with dual polarization receivers system, and a surface-coupled 1.6 GHz GSSI single transceiver/receiver system. The PulseEkko

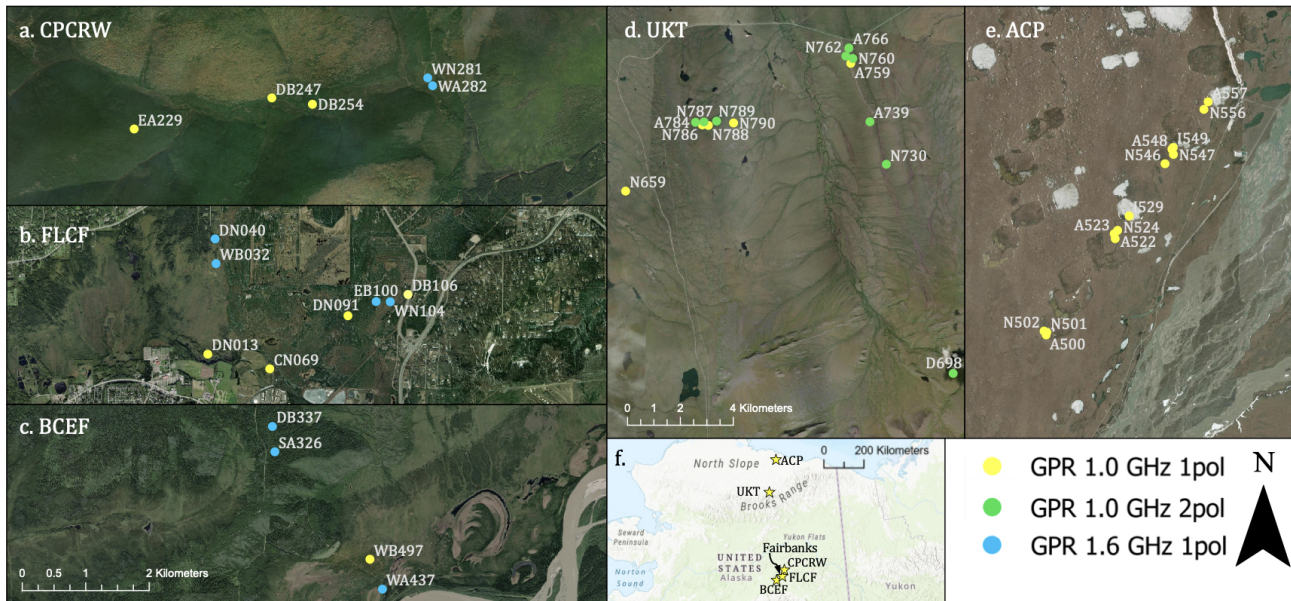


Figure 1. Ground surveys at the (a) Caribou/Poker Creek Research Watershed (CPCRW), (b) Farmers Loop/Creamer's Field (FLCF), (c) Bonanza Creek Experimental Forest (BCEF), (d) Upper Kuparuk-Toolik (UKT), and (e) Arctic Coastal Plain (ACP) field sites. (f) Map inset depicts the locations of the five field sites within Alaska. Imagery: Esri | Powered by Esri.

Pro systems have a 6 dB bandwidth of 500–1500 MHz, whereas the GSSI system has a 6 dB bandwidth of 800–2400 MHz. Each GPR used a GNSS system to provide locations for collected traces: the air-coupled PulseEKKO Pro used a Geode dGPS system (± 0.5 m accuracy), the two sled-coupled PulseEKKO Pro GPRs used Emlid RS2 rovers with Emlid RS2 bases located nearby for post-kinematic processing (± 0.5 m accuracy), and the sled-coupled GSSI GPR used a mapping-grade GPS system (± 3 m accuracy). In Fig. 1, each transect is marked by the associated GPR system.

For the three surface-coupled GPR surveys, the GPR was pulled across the surface of the snowpack in a sled, whereas the air-coupled GPR was carried by two people above the snow surface. GPR systems were operated in the common-offset configuration and we took care not to disturb the snowpack immediately below the GPR transect. Transect lengths ranged from 3–12 m. Methods for deriving GPR snow depths are provided in Sect. 3.2. Following GPR data collection, the snow along the full length of the transect was excavated and snowpack thicknesses, which excluded any void spaces or tree branches or logs in the snowpack, were measured at 0.25–1 m intervals. These snowpack thickness observations are unique, as typical in situ snow depths are measured with little-to-no knowledge of void spaces within the snowpack. Typical in situ snow depths are measured by using the probe to identify the ground, which has a large range of potential conditions (e.g., soft and mossy, hard and frozen, brushy) that can be challenging to interpret based on the ground-feel alone. The excavated snow depths are thus more representative of the true snowpack thickness, as demonstrated re-

cently by Stuefer et al. (2025). Pictures and/or video recordings were acquired for each transect and detailed notes were taken on vegetation and ground conditions. An example photomosaic of an excavated boreal forest transect is provided in Fig. 2. Each survey was completed within 15 m of a snow pit, wherein measurements of snow depth, snow density, SWE, and snow temperature were collected. In total, 17 surveys were collected at the boreal forest field sites and 27 surveys were collected at the tundra field sites on the North Slope.

At each field site, snow-on airborne lidar surveys were collected during the campaign and snow-off airborne lidar surveys were collected during the following summer. Snow-on and snow-off lidar surveys were used to generate 0.5 m snow depth and canopy height models (Larsen, 2024). We note that lidar-derived snow depths based on acquisitions that occurred before or after ground surveys have increased uncertainty due to either a changed snow surface (i.e., accumulation, compaction, redistribution) between the lidar flights and ground surveys or snow disturbance caused by the ground observations that preceded lidar flights ($n = 20/44$). Further processing details for the lidar snow depths are provided in Larsen (2024). A list of lidar and ground survey dates is provided in Table 1 and snow accumulation measurements for every day of the campaign are provided in Table S1 in the Supplement.

3.2 Ground-Penetrating Radar Processing and Sources of Snow Depth Uncertainty

For GPR systems, the transceiver emits a signal that transmits through the snowpack and reflects off boundaries of contrast-

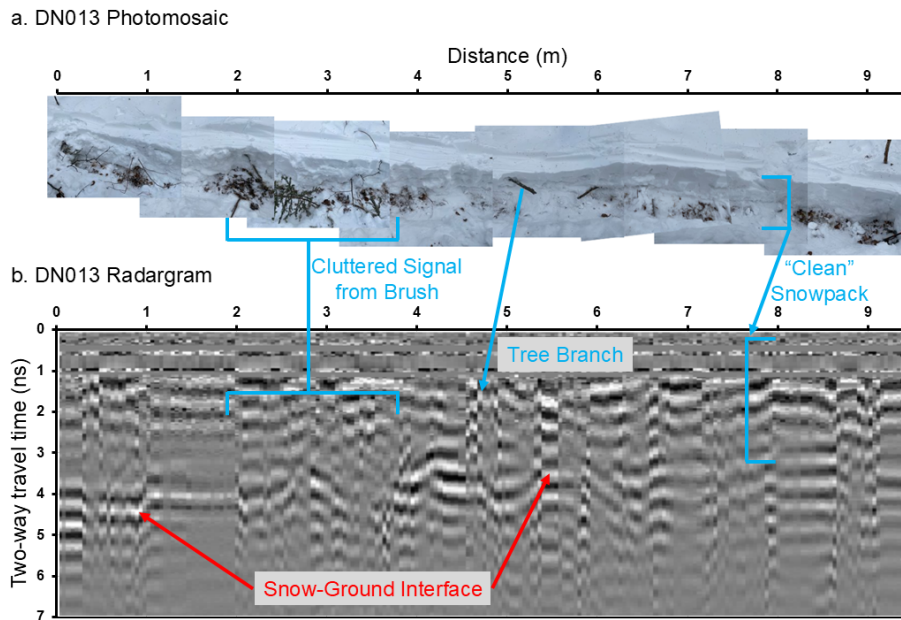


Figure 2. (a) Photomosaic and corresponding (b) radargram of the 9.5 m long DN013 transect from 7 March 2023 in Farmers Loop/Creamers Field. Annotations illustrate the complexities of GPR collection in the dense brush of boreal forests. In particular, we show the signal clutter caused by intra-snowpack vegetation, signal ringing that results from tree branches or tree trunks, snow stratigraphy in areas without vegetation (“clean” snowpack), and the location of the snow-ground interface, which ranges from ~ 4 ns near 0 m distance to ~ 3 ns near 9 m distance.

Table 1. Summary of field and airborne survey dates.

	Field Site	Snow-On Lidar Flight Date	Ground Survey Date	Transects (n)
Tundra	Arctic Coastal Plain	10 March 2023	11–14 March 2023	13
Tundra	Upper Kuparuk-Toolik	13 March 2023	8–11, 15 March 2023	14
Boreal Forest	Farmers Loop/Creamers Field	11 March 2023	7–11, 13 March 2023	8
Boreal Forest	Bonanza Creek Experimental Forest	11 March 2023	10, 13–15 March 2023	4
Boreal Forest	Caribou/Poker Creek Research Watershed	11 March 2023	8–9, 11, 14 March 2023	5

ing dielectric permittivities (e.g., vegetation, snow stratigraphy, the snow-ground interface). The receiver then records the amplitude and two-way travel times (twtt) of these reflections. Radargrams were processed to a trace spacing of ~ 0.10 m. We provide an example of a boreal forest radargram in Fig. 2. Exported twtt of the snow-ground interface, typically identified as the first reflection at depth with the highest amplitude that is spatially coherent, were manually selected for all single-polarization GPR datasets (e.g., McGrath et al., 2019). For the dual-polarization GPR dataset, twtt was obtained by utilizing the coherent reflection between the two receivers (further details provided in Meehan et al., 2024). The twtt can be converted to snow depth with an estimate of the snowpack radar velocity (v_s Daniels, 2004)

$$v_s = \frac{c}{\sqrt{\epsilon_s}}, \quad (1)$$

where c is the speed of electromagnetic energy in a vacuum and ϵ_s is the dielectric permittivity of the snowpack. Snow-

pack conditions were dry during our surveys, thus, the relative permittivity can be approximated from the bulk snow density (ρ_s) through an empirical relation (Kovacs et al., 1995)

$$\sqrt{\epsilon_s} = 1 + 0.845 \frac{\rho_s}{1000}. \quad (2)$$

Snow density was sampled in snow pits adjacent to the surveyed transects using 1000 cm³ wedge samplers at 10 cm intervals along two columns in the snow pit. If density measurements differed by more than 10 % for a single layer, a third measurement was acquired. For layers with three measurements, we excluded the measurement with the largest difference. We then calculated bulk snow densities as the column average. Finally, snow depth (D_s) is calculated as

$$D_s = v_s \frac{twtt}{2}. \quad (3)$$

GPR surveys have several sources of uncertainty. GNSS positioning was estimated as ± 0.5 –3 m horizontal accuracy

at the boreal forest sites and ± 0.5 m at the Arctic tundra sites, which could complicate the comparison between GPR and lidar snow depths. GPR-derived snow depths may be reduced by up to 0.07 m due to removal and/or compaction of snow as the sled travels across the surface. Finally, site-specific ground conditions may add uncertainty to the GPR snow depths. A few examples include: (1) snow depths may be overestimated because of the presence of void spaces within the snowpack caused by vegetation, (2) snow depths may be underestimated when a dense layer of vegetation obscures the true bottom of the snowpack (e.g., a buried bent-over tree), and (3) snow depths may be overestimated if the radar signal penetrates into frozen soil without a strong reflection at the snow-ground interface.

3.3 Evaluation of GPR and Lidar Snow Depths

We extracted the lidar snow depths ($0.5 \text{ m} \times 0.5 \text{ m}$ resolution) along each surveyed transect based on the GNSS coordinates recorded by the GPR. We aligned the excavated depth locations with the GPR depth locations based on field measurements, resulting in a high-quality co-registration between the GPR and the excavated depths. However, the co-registration between the lidar data and the transect surveys are subject to the GNSS uncertainty listed above. GPR, lidar, and excavated depths were then compared as individual profiles to evaluate any systematic differences. We calculated the mean and standard deviation of snow depth for the GPR, lidar, and in-situ measurements from each transect to estimate the overall root mean squared error (RMSE), bias, and Pearson's correlation coefficient (r) between measurement techniques in both the tundra and boreal forest sites. Although both GPR and lidar snow depths likely contain errors and biases, we primarily emphasize bias in the results and discussion because the two are difficult to untangle due to the complex conditions in which these data were collected. Finally, lidar-derived vegetation heights were extracted along each transect in the boreal forest to determine whether accuracy was related to lidar-derived vegetation height.

4 Results

4.1 Boreal Forest Transects

At boreal forest sites, GPR mean snow depths overestimated excavated mean snow depths for 12 of 17 transects, whereas lidar mean snow depths underestimated excavated mean snow depths for 14 of 17 transects (Table S2, Fig. 3). Large differences (> 0.20 m) between GPR and excavated depths occurred where sub-snow shrubs or tree branches caused void spaces in the snowpack (e.g., Fig. 3g, i), but close agreement was observed for the transect in the agricultural field where only crop stubble was present below the snowpack (Fig. 3b) and for transects below black spruce canopy (e.g., Fig. 3n–p). The average residual between GPR and exca-

vated depths was $+0.06$ m (9 % of mean excavated depth) and the average residual between lidar and excavated depths was -0.12 m (16 % of overall mean excavated depth) when field surveys occurred after lidar acquisitions (Table S2). For these surveys, the lidar profile either mostly mimicked the excavated depths and agreed within ± 0.07 m (e.g., Fig. 3j, p), or the lidar profile failed to capture both the spatial patterns and exhibited reduced accuracy when compared to the excavated depths (e.g., Fig. 3h, l). The lidar snow depth bias worsened to -0.16 m (24 % of mean excavated depth; Table S2) when surveys performed before the lidar survey date were included in the comparison. We visually inspected the boreal forest lidar snow depth rasters to verify the presence of all transects excavated before the 11 March lidar survey and we found that excavation activities clearly influenced five of these surveys. These transects are shown in Fig. 3b, d, e, f, and n, illustrating how sample timing can severely bias direct comparisons between field and remote sensing-based depth estimates.

Of the three boreal forest field sites, CPCRW yielded the lowest mean GPR residual ($+0.03$ m), whereas BCEF yielded the highest mean residual ($+0.11$ m). Three of the five CPCRW transects were performed below black spruce canopy, where mosses are the dominant substrate and shrub canopy is sparse, whereas shrubs and tussocks dominate the ground below BCEF transects. FLCF surveys (mean GPR residual = $+0.06$ m) were performed primarily below mixed deciduous/coniferous canopy and contained various shrubs, saplings, and tree branches within the snowpack. Compared to GPR, mean lidar residuals exhibited the opposite canopy-driven trend; BCEF surveys yielded the lowest mean residuals (-0.10 m) and FLCF/CPCRW yielded the highest mean residuals (-0.19 and -0.15 m). However, we note that three of four BCEF surveys were performed after lidar collection, whereas eight of 13 surveys at FLCF/CPCRW were performed before lidar collection (Table S2). Overall, we calculated an r of 0.55 and RMSE of 0.14 m for GPR snow depths and an r of 0.51 and RMSE of 0.22 m for lidar snow depths at the boreal forest field sites (Fig. 4a–b). The best Pearson's correlation coefficient, but highest RMSE was observed for the lidar vs. GPR comparison ($r = 0.66$, RMSE = 0.26 m; Fig. 4c).

4.2 Tundra Transects

Vegetation structure was less complex at the Arctic tundra sites than at the boreal forest sites. At ACP, surveys had grassy ground cover (11 surveys with grass heights of 0.05–0.20 m) or ground ice (two surveys; Fig. 5i, m), whereas tussocks (four surveys with tussock heights of 0.08–0.25 m) and shrubs (four surveys with shrub heights < 0.30 m) were the predominant ground cover at UKT. Based on the excavated depths, both mean GPR residuals (ACP = $+0.03 \pm 0.04$ m; UKT = $+0.01 \pm 0.10$ m; Tables S3–S4, Figs. 5–6) and the overall performance metrics ($r = 0.87$;

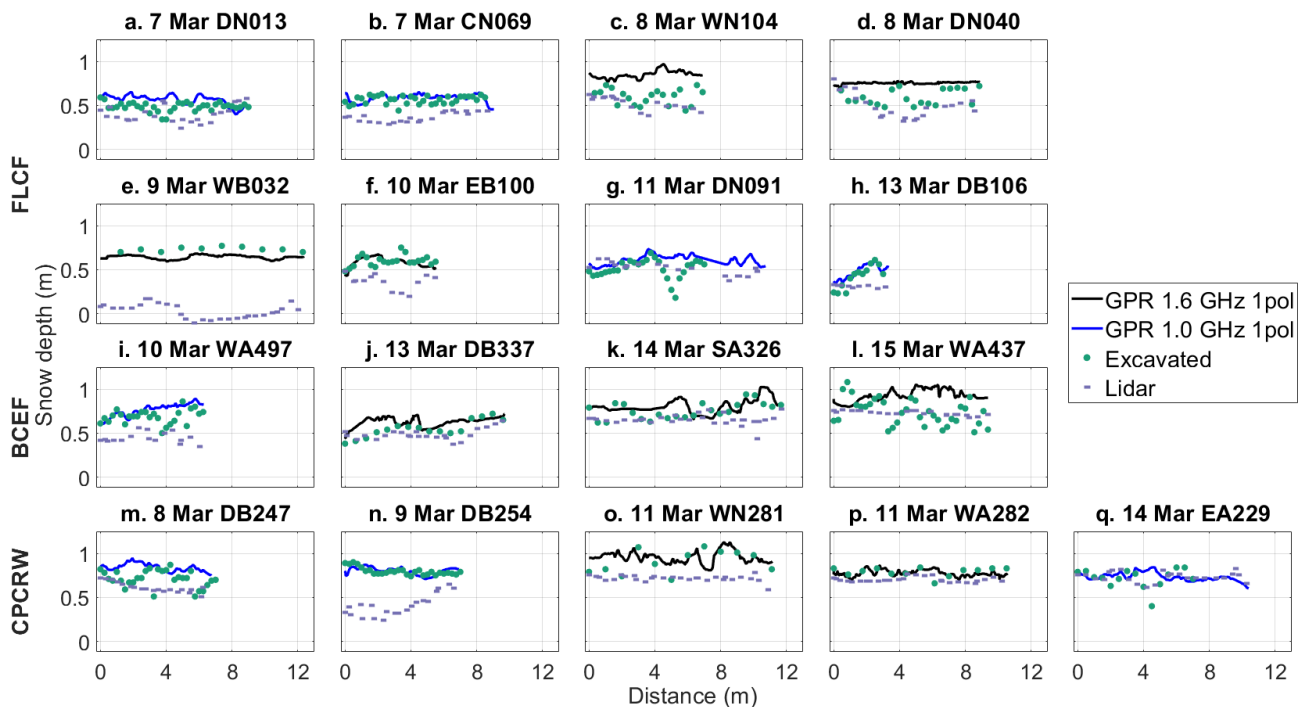


Figure 3. Snow depth profiles at the boreal forest for the (a–h) Farmer’s Loop/Creamer’s Field (FLCF), (i–l) Bonanza Creek Experimental Forest (BCEF), and (m–q) Caribou/Poker Creek Research Watershed (CPCRW) field sites. GPR snow depth profiles were collected by the 1.6 GHz GPR system and the 1.0 GHz GPR system. Subplots are labeled by transect numbers. Airborne lidar surveys were conducted at all three sites on 11 March 2023.

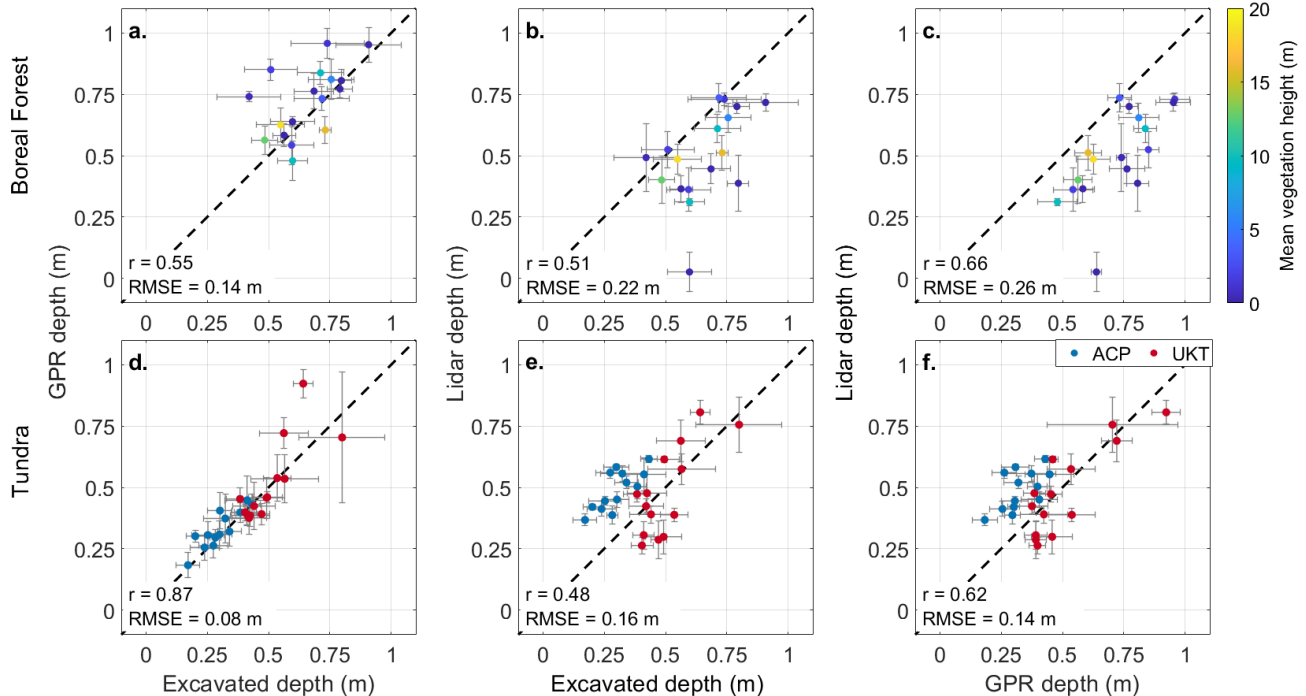


Figure 4. Comparisons at the boreal forest (a–c) and tundra sites (d–f) between (a, d) GPR and excavated depths, (b, e) lidar and excavated depths, and (c, f) lidar and GPR depths. The mean values are plotted with error bars showing the standard deviation. Points in (a)–(c) are colored by mean lidar-derived vegetation height, which represents the canopy height in forest cover or the shrub/grass height in meadows. Points in (d)–(f) are colored by field site. Sites: ACP, Arctic Coastal Plain; UKT, Upper Kuparuk-Toolik.

RMSE = 0.08; Fig. 4d) improved at the Arctic tundra sites relative to the boreal forest sites.

Compared to the boreal forest sites, the lidar snow depths from the Arctic tundra sites yielded a comparable Pearson's correlation coefficient, but an improved RMSE ($r = 0.48$; RMSE = 0.16 m; Fig. 4e). Despite having more complex ground conditions than ACP, UKT yielded the lowest mean lidar residual (ACP = $+0.19 \pm 0.05$ m; UKT = -0.02 ± 0.12 m; Tables S3–S4, Figs. 5–6). All ACP lidar profiles exhibited poor magnitude agreement with the excavated depths. Despite this, several of these profiles exhibited spatial patterns that were similar to the excavated depth profiles (Fig. 5c, f, i, m). Notably, all ACP surveys were performed after the lidar flight, whereas 13 of 14 UKT surveys preceded the lidar flight (Table 1). We visually inspected the transects in the UKT lidar snow depth raster and observed that only five transects were influenced by snow excavation (Fig. 6h–j, l–m).

5 Discussion

5.1 GPR and Lidar Snow Depth Uncertainty in Boreal Forest and Arctic Tundra Environments

We found that GPR captured snow depth variability in both boreal forest and Arctic tundra environments over length scales > 0.5 m, but we observed larger uncertainty over shorter length scales (< 0.5 m), likely due to the large sensor footprint (~ 1.5 m radius for a snow depth of 0.6 m; e.g., Daniels, 2004). GPR snow depths exhibited a modest positive bias ($+0.06$ m) relative to excavated depths in the boreal forest and a smaller positive bias in the Arctic tundra (overall mean residuals = $+1$ – 3 cm; Tables S2, S3). While it is possible that a portion of the observed GPR bias could be explained by differences between the GPR and excavated depth measurement footprints, we largely attribute the positive biases to discontinuous vegetation-induced void spaces at the base and within the snowpack (e.g., Fig. 2; Berezovskaya and Kane, 2007). Vegetation was dense and complex in the boreal forest, resulting in cluttered radargrams that were difficult to interpret, whereas Arctic tundra sites had less complex vegetation and better-defined ground reflectors.

Lidar at ACP was expected to have the highest agreement with excavated depths because the lidar surveys were conducted before the snowpack was disturbed. Instead, ACP lidar exhibited a $+0.19$ m average bias and failed to reproduce fine-scale snow depth patterns (e.g., Fig. 5a–b), despite having relatively simpler ground conditions at the time of the surveys. We attribute this to a strip alignment issue in the ACP bare earth elevation model collected in August 2022, which results in linear striping in the snow depths aligned with the lidar swaths. All ground surveys happened to be conducted within a single swath that exhibited higher snow

depths (Fig. 7), which provides the likely explanation for the observed ACP bias in the snow depths.

Although UKT lidar exhibited lower mean bias, it also did not reproduce fine-scale snow depth patterns (e.g., Fig. 6e–f). Both ACP and UKT received < 0.06 m of snow depth accumulation between ground-based and airborne surveys (Table S1). Based on field observations, blowing snow and wind redistribution (e.g., Pomeroy and Li, 2000) likely caused the poor spatial pattern agreement between excavated depth and lidar depth profiles. Seasonal thaw, which has been observed to drive subsidence up to 0.05 m in this region (Chen et al., 2020), may also contribute, but is challenging to quantify with available observations.

Lidar at the boreal forest also exhibited higher uncertainties, yielding an RMSE that was nearly half of the average measured snow depth. However, May et al. (2025) demonstrated that the RMSE could be reduced to 0.12 m at CPCRW by removing anomalous snow depths and areas with anomalous snow depth patterns. Uncertainties tended to be higher for taller vegetation heights (> 5 m; Fig. 4b), although we note a large range of accuracy for lower vegetation heights (< 5 m). This weaker agreement could be due to one or more of four primary factors: (1) snow disturbance due to ground surveys caused errors within the lidar retrieval method, (2) differences in canopy structure between summer and winter acquisitions (e.g., bent-over trees from snow burden), (3) signal penetration through the dense canopy may be problematic for the method (e.g., Hopkinson et al., 2004), or (4) GNSS location uncertainty between the lidar and excavated depths. Despite the higher uncertainty for the lidar snow depths, the lidar coverage is spatially continuous and complete over the field sites, a clear advantage over the GPR measurements.

5.2 Implications for SnowEx23 GPR and Lidar Datasets

Although we identified a clear bias for GPR in the boreal forest, it appears that this bias exhibited some dependence upon the land cover, but we were unable to fully evaluate this point. Further work, potentially through a depth probe-GPR evaluation, is needed to identify systematic biases within the boreal forest for GPR operation.

ACP lidar snow depths appear to be affected by swath alignment artifacts, which users should be aware of before using the dataset. If the identified bias is removed from the lidar swath by simple subtraction, the ACP lidar RMSE improves from 0.20 to 0.05 m. However, the remaining lidar swaths may be challenging to correct given the lack of independent in situ observations in these swaths. At UKT, lidar snow depths exhibited low bias and relatively high accuracy, whereas lidar snow depths at the boreal forest sites exhibited a substantial positive bias. Fair et al. (2025) evaluated ICESat-2 lidar snow depths at UKT and FLCF using the airborne lidar snow depths and found better ICESat-2 perfor-

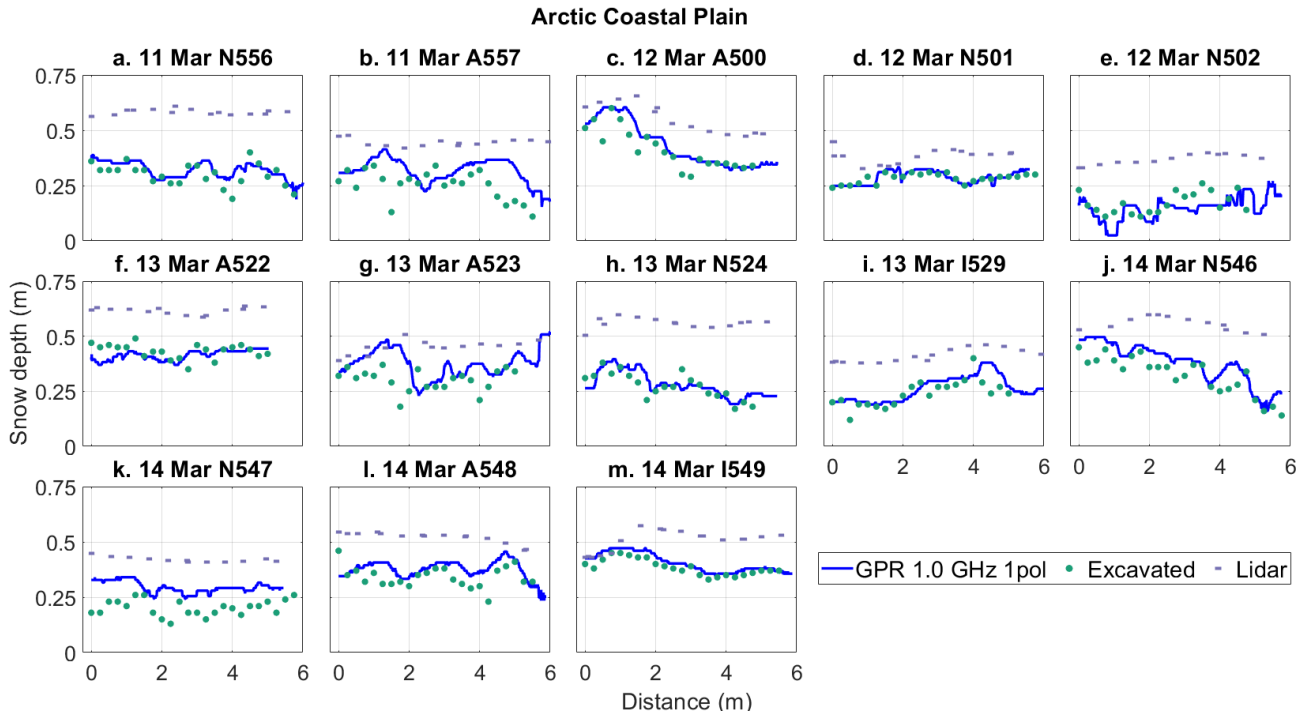


Figure 5. Snow depth profiles at the Arctic Coastal Plain tundra field site organized by date and transect number. GPR snow depth profiles were collected by the single-polarization 1.0 GHz GPR system. Airborne lidar survey was conducted on 10 March 2023.

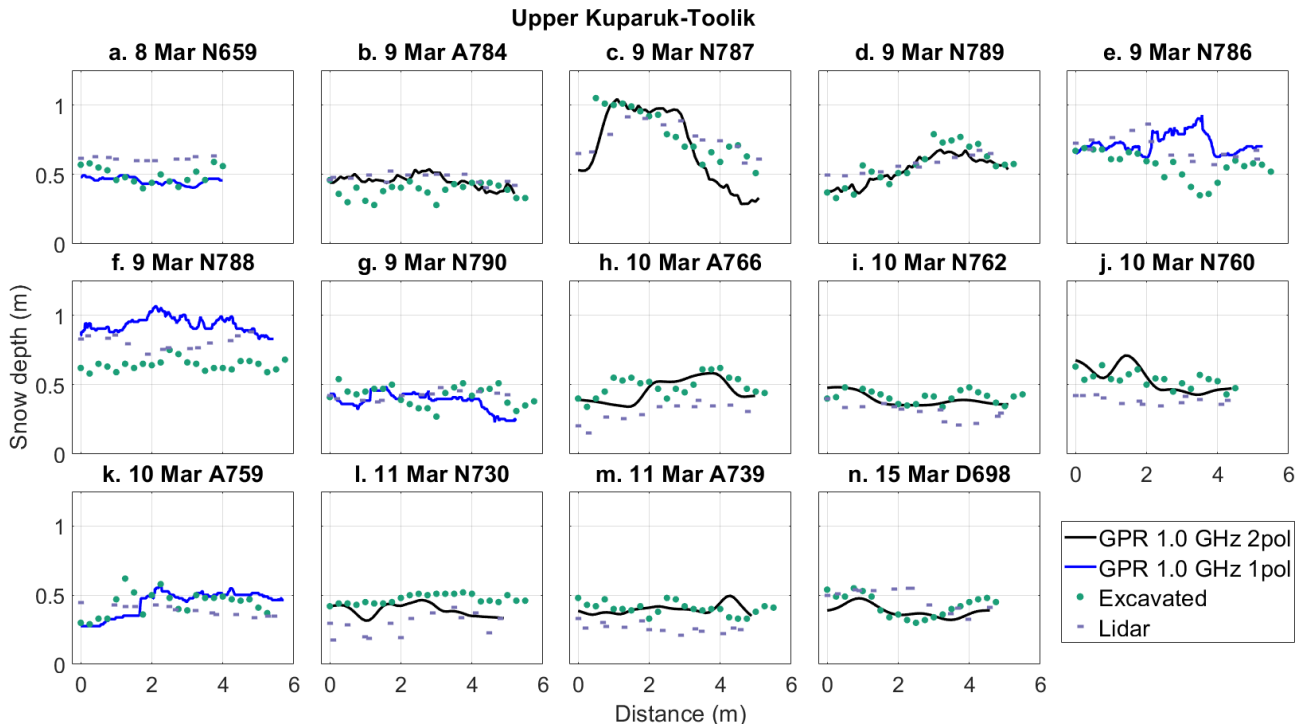


Figure 6. Snow depth profiles at the Upper Kuparuk-Toolik tundra field site organized by date and transect ID. GPR snow depth profiles were collected by the single-polarization 1.0 GHz GPR system and the dual-polarization 1.0 GHz GPR system. Airborne lidar survey was conducted on 13 March 2023.

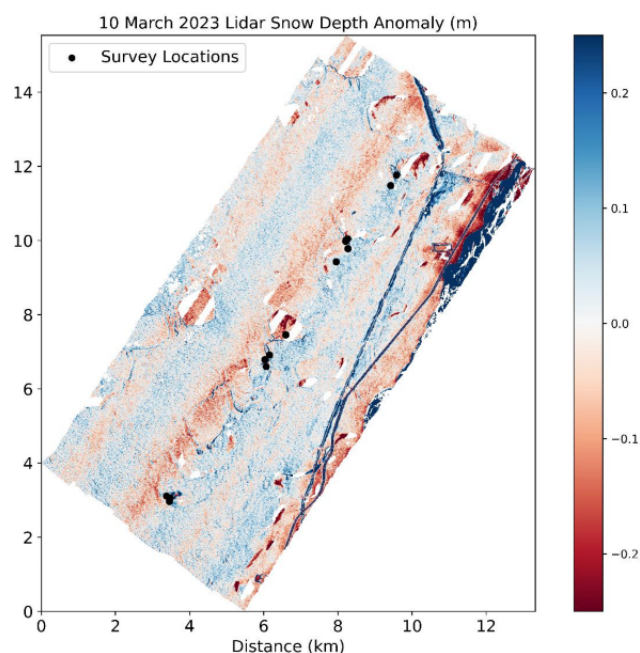


Figure 7. Lidar snow depth anomalies at ACP with snow depth anomaly saturated between -0.25 and $+0.25$ m to illustrate the linear lidar artifacts oriented southwest to northeast. All GPR transect locations are located within a single swath of the scene.

mance at UKT ($r^2 = 0.84$ – 0.92) than at FLCF ($r^2 = 0.14$ – 0.58), further highlighting the boreal forest complexities. In the forests, the lidar snow depth bias is directly related to potential void spaces caused by shrub canopy interception and a lack of photon penetration below canopy and underbrush. In the Arctic tundra, lidar snow depths may be influenced by seasonal thaw cycles. Given the magnitude of snow disturbance associated with in situ surveys, we expect poor agreement between snow pit/excavated measurements and lidar measurements when the field survey preceded the lidar flight (e.g., Fig. 3e, n).

6 Conclusions

Snow is a critical component of the hydrology and ecology of high-latitude terrestrial environments, but distributed snow depths are difficult to measure at high spatial resolution. As part of the NASA SnowEx March 2023 campaign, spatially distributed L-band center-frequency GPR and airborne lidar data were collected and we evaluated snow depth retrievals at the boreal forest and Arctic tundra sites. Biases were observed for both methods and in both environments. GPR surveys yielded accurate snow depths, but with lower variability along the profile which was likely caused by the much larger footprint of the radar signal. GPR, particularly when operated at or near the snowpack surface, is less sensitive to vegetation and snowpack void spaces than the air-

borne lidar snow-on/off DEM differencing method. The timing of the lidar flights relative to ground surveys complicated our evaluation, but we noted lower accuracy in the boreal forest that may have been caused by vegetation preventing the lidar pulse from reaching the bare earth. Although lidar yielded accurate snow depths at the UKT site, we identified vertical alignment issues that contributed to a large positive bias at ACP (bias = $+0.19$ m). The complex surface conditions of the boreal forest and tundra regions challenge established snow observing methods, warranting careful consideration when using these to evaluate novel remote sensing approaches.

Data availability. Boreal Forest GPR transects (Bonnell et al., 2025, <https://doi.org/10.5067/3X5Q3X7Y87U3>), Arctic Tundra dual polarization (Meehan and Rowland, 2024, <https://doi.org/10.5067/TSU0U7L4X2UW>) and single polarization (Webb, 2024, <https://doi.org/10.5067/H3D9IT1W6JT6>) GPR transects, lidar data (Larsen, 2024, <https://doi.org/10.5067/BV4D8RRU1H7U>), and snow pits (Mason et al., 2024, <https://doi.org/10.5067/SJZ90KNPKCYR>) are archived with the NSIDC DAAC. Creamer’s Field SNOTEL data are available at <https://wcc.sc.egov.usda.gov/nwcc/site?sitenum=1302> (last access: 1 May 2025). NOAA AK Deadhorse 3 S weather station data are available at <https://www.ncei.noaa.gov/access/crn/sensors.htm?stationId=1793> (last access: 1 May 2025).

Supplement. The supplement related to this article is available online at <https://doi.org/10.5194/tc-20-2169-2026-supplement>.

Author contributions. Conceptualization: DM, HPM, CV, KHG, RB, TM, RW. Data Curation: KHG, CL, RW, TM, MM, RB, DM, BB. Analysis: KHG, RB, TM, RW. Funding Acquisition: DM, CV, HPM, RW, RB, BB, TM, KHG. Investigation: all authors. Methodology: KHG, DM, TM, RW, RB. Visualization: KHG, RB. Writing – Original Draft Preparation: KHG, RB, DM. Writing – Review and Editing: all authors.

Competing interests. At least one of the (co-)authors is a member of the editorial board of *The Cryosphere*. The peer-review process was guided by an independent editor, and the authors also have no other competing interests to declare.

Disclaimer. Any use of trade, firm, or product names is for descriptive purposes only and does not imply endorsement by the U.S. Government.

Publisher’s note: Copernicus Publications remains neutral with regard to jurisdictional claims made in the text, published maps, institutional affiliations, or any other geographical representation in this paper. The authors bear the ultimate responsibility for providing appropriate place names. Views expressed in the text are

those of the authors and do not necessarily reflect the views of the publisher.

Acknowledgements. Kajsa Holland-Goon was supported by the Colorado State University Honors program. Randall Bonnell was supported by NASA FINESST award 80NSSC20K1624 and the U.S. Geological Survey Mendenhall Postdoctoral Fellowship Program. Daniel McGrath, Hans-Peter Marshall, and Ryan Webb were supported by NASA THP award 80NSSC22K1113. We thank E. Baker, H. Flynn, and N. Latysh for providing insightful comments which improved the clarity of this paper.

Financial support. This research has been supported by the National Aeronautics and Space Administration (grant nos. 80NSSC20K1624 and 80NSSC22K1113).

Review statement. This paper was edited by S. McKenzie Skiles and reviewed by Matthew Sturm and Andrea Vergnano.

References

- Aitchison, C. W.: Winter energy requirements of soricine shrews, *Mammal Rev.*, 17, 25–38, <https://doi.org/10.1111/j.1365-2907.1987.tb00046.x>, 1987.
- Benson, C. S.: Polar regions snow cover, *Physics of Snow and Ice: Proceedings, Sapporo, Japan, 1966*, 1039–1063, 1967.
- Benson, C. S. and Sturm, M.: Structure and wind transport of seasonal snow on the Arctic slope of Alaska, *Ann. Glaciol.*, 18, <https://doi.org/10.3189/S0260305500011629>, 1993.
- Berezovskaya, S. and Kane, D. L.: Measuring snow water equivalent for hydrological applications: part 1, accuracy observations, 16th International Northern Research Basins Symposium and Workshop, Petrozavodsk, Russia, 27 August–2 September 2007, 29–35, 2007.
- Bonnell, R., McGrath, D., Detre, A., and Holland-Goon, K.: SnowEx23 Mar23 IOP CSU 1GHz Ground Penetrating Radar Raw, Version 1, NASA National Snow and Ice Data Center Distributed Active Archive Center [data set], <https://doi.org/10.5067/3X5Q3X7Y87U3>, 2025.
- Chen, J. Wu, Y., O'Connor, M., Cardenas, M. B., Schaefer, K., Michaelides, R., and Kling, G.: Active layer freeze-thaw and water storage dynamics in permafrost environments inferred from InSAR, *Remote Sens. Environ.*, 248, 112007, <https://doi.org/10.1016/j.rse.2020.112007>, 2020.
- Daniels, D. J. (Ed.): *Ground Penetrating Radar, Volume 1*, The Institution of Electrical Engineers, ISBN 13:978-0863413605, 2004.
- Duquette, L. S.: Snow Characteristics along Caribou Trails and within Feeding Areas during Spring Migration, Arctic, 41, 143–144, <https://journalhosting.ucalgary.ca/index.php/arctic/article/view/64760/48674> (last access: 1 January 2026), 1988.
- Eppler, J., Rabus, B., and Morse, P.: Snow water equivalent change mapping from slope-correlated synthetic aperture radar interferometry (InSAR) phase variations, *The Cryosphere*, 16, 1497–1521, <https://doi.org/10.5194/tc-16-1497-2022>, 2022.
- Fair, Z., Vuyovich, C., Neumann, T. A., Larsen, C. F., Stuefer, S. L., Mason, M., and May, L.: Characterizing ICESat-2 Snow Depths Over the Boreal Forests and Tundra of Alaska in Support of the SnowEx 2023 Campaign, *Water Resour. Res.*, 61, e2024WR039076, <https://doi.org/10.1029/2024WR039076>, 2025.
- Hopkinson, C., Sitar, M., Chasmer, L., and Treitz, P.: Mapping snowpack depth beneath forest canopies using airborne lidar, *Photogramm. Eng. Rem. S.*, 70, 323–330, <https://doi.org/10.14358/PERS.70.3.323>, 2004.
- Jorgensen, T., Yoshikawa, K., Kanevskiy, M., Shur, Y., Romanovsky, V., Marchenko, S., Grosse, G., Brown, J., and Jones, B.: Permafrost Characteristics of Alaska [map] https://permafrost.gi.alaska.edu/sites/default/files/AlaskaPermafrostMap_Front_Dec2008_Jorgensen_et_al_2008.pdf (last access: 1 May 2025), 2008.
- Kelsey, K. C., Pedersen, S. H., Leffler, A. J., Sexton, J. O., Feng, M., and Welker, J. M.: Winter snow and spring temperature have differential effects on vegetation phenology and productivity across Arctic plant communities, *Glob. Change Biol.*, 27, 1572–1586, <https://doi.org/10.1111/gcb.15505>, 2021.
- Kovacs, A., Gow, A. J., and Morey, R. M.: The in-situ dielectric constant of polar firn revisited, *Cold Reg. Sci. Technol.*, 23, 245–256, [https://doi.org/10.1016/0165-232X\(94\)00016-Q](https://doi.org/10.1016/0165-232X(94)00016-Q), 1995.
- Larsen, C.: SnowEx23 Airborne Lidar-Derived 0.25M Snow Depth and Canopy Height, Version 1, NASA National Snow and Ice Data Center Distributed Active Archive Center [data set], <https://doi.org/10.5067/BV4D8RRU1H7U>, 2024.
- Mason, M., Vuyovich, C. M., Stuefer, S., Elder, K., Vas, D., Marshall, H., and Durand, M.: SnowEx23 Mar23 Snow Pit Measurements, Version 1, NASA National Snow and Ice Data Center Distributed Active Archive Center [data set], <https://doi.org/10.5067/SJZ90KNPKCYR>, 2024.
- May, L. D., Stuefer, S. L., Goddard, S. D., and Larsen, C. F.: Analyzing vegetation effects on snow depth variability in Alaska's boreal forests with airborne lidar, *The Cryosphere*, 19, 3477–3492, <https://doi.org/10.5194/tc-19-3477-2025>, 2025.
- McGrath, D., Webb, R., Shean, D., Bonnell, R., Marshall, H.-P., Painter, T. H., Molotch, N. P., Elder, K., Hiemstra, C., and Brucker, L.: Spatially Extensive Ground-Penetrating Radar Snow Depth Observations During NASA's 2017 SnowEx Campaign: Comparison With In Situ, Airborne, and Satellite Observations, *Water Resour. Res.*, 55, 10026–10036, <https://doi.org/10.1029/2019WR024907>, 2019.
- Meehan, T. G. and Rowland, T.: SnowEx23 CRREL Ground Penetrating Radar, Version 1, NASA National Snow and Ice Data Center Distributed Active Archive Center [data set], <https://doi.org/10.5067/TSU0U7L4X2UW>, 2024.
- Meehan, T. G., Hojatimalekshah, A., Marshall, H.-P., Deeb, E. J., O'Neil, S., McGrath, D., Webb, R. W., Bonnell, R., Raleigh, M. S., Hiemstra, C., and Elder, K.: Spatially distributed snow depth, bulk density, and snow water equivalent from ground-based and airborne sensor integration at Grand Mesa, Colorado, USA, *The Cryosphere*, 18, 3253–3276, <https://doi.org/10.5194/tc-18-3253-2024>, 2024.
- Meredith, M., Sommerkorn, M., Cassotta, S., Derksen, C., Ekaykin, A., Hollowed, A., Kofinas, G., Mackintosh, A., Melbourne-Thomas, J., Muelbert, M. M. C., Ottersen, G., Pritchard, H., and Schuur, E. A. G.: Polar Regions. IPCC Special Report on

- the Ocean and Cryosphere in a Changing Climate, 203–320, <https://doi.org/10.1017/9781009157964.005>, 2019.
- NASA Earth Observatory: Forest on the Threshold, [blog post], https://earthobservatory.nasa.gov/features/BorealThreshold/boreal_threshold4.php (last access: 1 May 2025), 2006.
- Obu, J., Westermann, S., Bartsch, A., Berdnikov, N., Christiansen, H. H., Dashtseren, A., Delaloye, R., Elberling, B., Etzelmüller, B., Kholodov, A., Khomutov, A., Kääb, A., Leibman, M. O., Lewkowicz, A. G., Panda, S. K., Romanovsky, V., Way, R. G., Westergaard-Nielsen, A., Wu, T., Yamkhin, J., and Zou, D.: Northern Hemisphere permafrost map based on TTOP modelling for 2000–2016 at 1 km² scale, *Earth-Sci. Rev.*, 193, 233–316, <https://doi.org/10.1016/j.earscirev.2019.04.023>, 2019.
- Penczykowski, R. M., Connolly, B. M., and Barton, B. T.: Winter is changing: Trophic interactions under altered snow regimes, *Food Webs*, 13, 80–91, <https://doi.org/10.1016/j.fooweb.2017.02.006>, 2017.
- Pedersen, S. H., Bentzen, T. W., Reinking, A. K., Liston, G. E., Elder, K., Lenart, E. A., Prichard, A. K., and Welker, J. M.: Quantifying effects of snow depth on caribou winter range selection and movement in Arctic Alaska, *Movement Ecology*, 9, 48, <https://doi.org/10.1186/s40462-021-00276-4>, 2021.
- Pomeroy, J. W. and Li, L.: Prairie and arctic areal snow cover mass balance using a blowing snow model, *J. Geophys. Res.-Atmos.*, 105, 26619–26634, <https://doi.org/10.1029/2000JD900149>, 2000.
- Pruitt Jr., W.: Some ecological aspects of snow, *Ecology of the Subarctic Regions: Proceedings of the Helsinki Symposium*, UNESCO, Helsinki, Finland, 1970, 83–99, <https://unesdoc.unesco.org/ark:/48223/pf0000004082> (last access: 1 January 2026), 1970.
- Stuefer, S. L., Hale, K., May, L. D., Mason, M., Vuyovich, C., Marshall, H. P., Vas, D., and Elder, K.: Snow depth measurements from Arctic tundra and boreal forest collected during NASA SnowEx Alaska Campaign, *Sci. Data*, 12, 919, <https://doi.org/10.1038/s41597-025-05430-w>, 2025.
- Vuyovich, C., Stuefer, S., Gleason, K., Durand, M., Marshall, H. P., Osmanoglu, B., Elder, K., Vas, D., Mason, M., Nolin, A., Youcha, E., Gelvin, A., Larsen, C., Pedersen, S., Hodgkinson, D., Deeb, E., and Boyd, D.: NASA SnowEx 2023 Experiment Plan [science plan], https://snow.nasa.gov/sites/default/files/users/user354/SNEX-Campaigns/2023/NASA_SnowEx_Experiment_Plan_2023_draft_20June2024.pdf (last access: 1 May 2025), 2024.
- Webb, R.: SnowEx23 University of Wyoming Ground Penetrating Radar, Version 1, NASA National Snow and Ice Data Center Distributed Active Archive Center [data set], <https://doi.org/10.5067/H3D9IT1W6JT6>, 2024.